Supporting Information

Direct Observations of Phase Distributions in Operating $LiFeSO_4F$ Battery Electrodes

Andreas Blidberg,[1] *Torbjörn Gustafsson,*[1] *Carl Tengstedt*[2] *Fredrik Björefors,*[1] *and William R. Brant*[1]*

[1]Department of Chemistry – Ångström Laboratory, Uppsala University, Box 538, SE-75121 Uppsala, Sweden

[2]Scania CV AB, SE-15187, Södertälje, Sweden

* Corresponding Author: william.brant@kemi.uu.se

Table of Contents

I. Calculation of electrode porosity

The electrode porosity was calculated from the total volume of the cast composite and the volume of a completely dense cast.

$$Electrode\ porosity = \frac{V_{void}}{V_{total}} = \frac{V_{measured} - V_{dense}}{V_{measured}}$$

The total volume was calculated by multiplying the thickness of the cast by its geometrical area. The volume of a dense electrode was calculated by dividing the mass of the cast composite by its average density (ρ_{cast}).

$$V_{dense} = \frac{m_{cast}}{\rho_{cast}}$$

ρ_{cast} is the sum of the different components' densities multiplied by their weight fractions (w_n):

$$\rho_{cast} = w_1\rho_{LiFeSO_4F} + w_2\rho_{PEDOT-TFSI} + w_3\rho_{binder} + w_4\rho_{carbon\ black}$$

$\rho_{LiFeSO4F}$ is 3.24 g/cm^3 from Rietveld refinement, $\rho_{carbon\ black}$ is 1.9 g/cm^3 and ρ_{binder} is 1.78 g/cm^3 according to data from the suppliers. The density of PEDOT-TFSI is assumed to be similar to the density of electropolymerized PEDOT-ClO_4, *i.e.* $\rho_{PEDOT-TFSI}$ is 1.65 g/cm^3.[2] The electrode formulation of $LiFeSO_4F$/PEDOT/carbon black/binder was equal to 70.0/10.5/8.0/11.5, which gave a density of 2.80 g/cm^3 for the cast composite.

II. Details regarding XRD and the Rietveld refinements

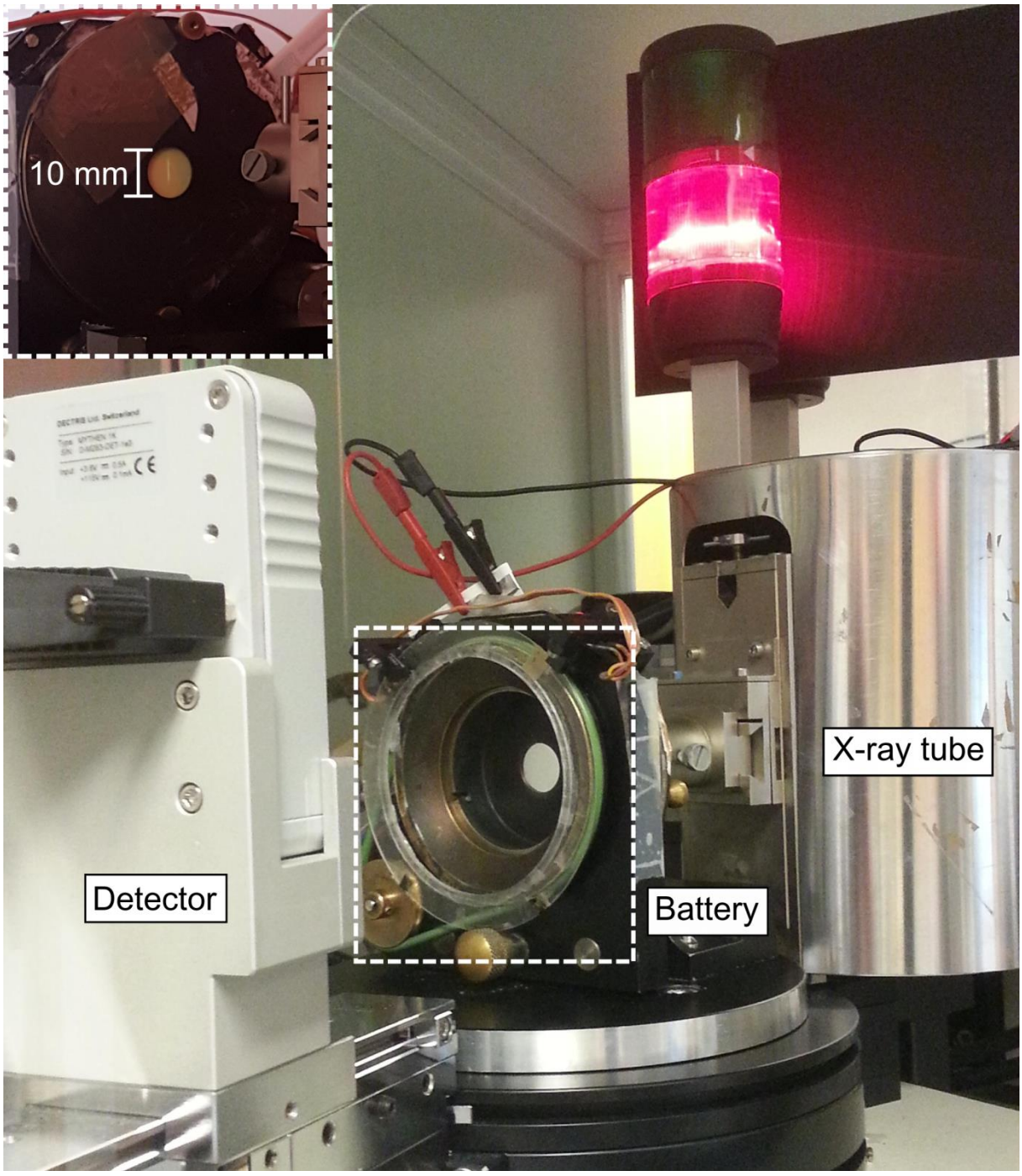

Figure S1. Image of the experimental set-up for *in operando* XRD. The position and size of the beam is shown using a flourescent strip in the inset.

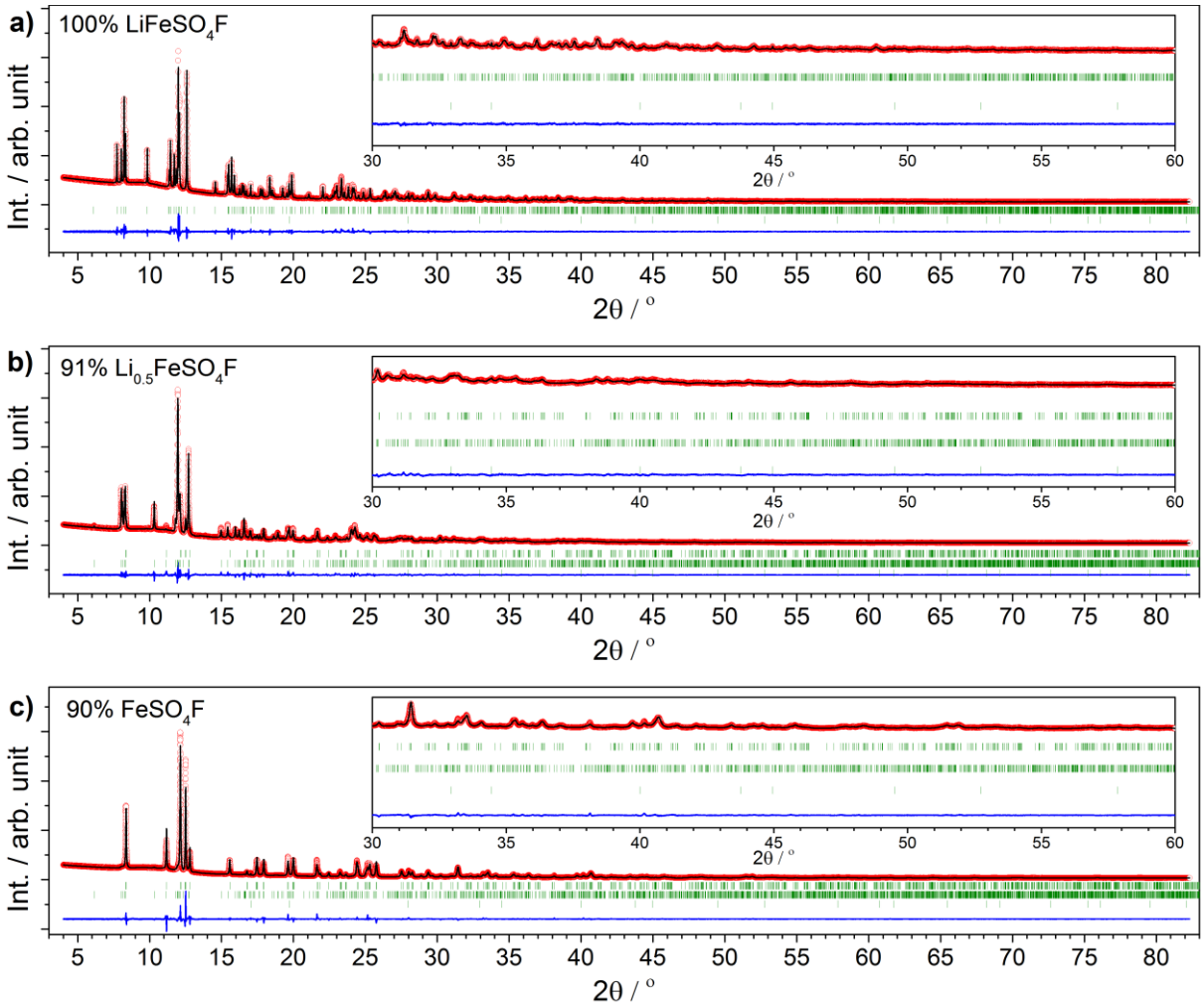

Figure S2. The entire synchrotron XRD data set and accompanying Rietveld refinement of references phases of a) $LiFeSO_4F$, b) $Li_{0.5}FeSO_4F$, and c) $FeSO_4F$. The Bragg positions (from top to bottom) correspond to in a) to $LiFeSO_4F$ and LiF, in b and c) to $FeSO_4F$, $Li_{0.5}FeSO_4F$ and LiF. The 30-60 ° 2θ regions are magnified in the insets.

Table S1. Agreement factors.

	$LiFeSO_4F$	**$Li_{1/2}FeSO4F$**	**$FeSO_4F$**
R_{Bragg}	3.68	3.87	3.59
R_p	2.61	3.03	3.18
R_{wp}	3.58	4.17	4.89
χ^2	6.65	10.4	16.3

Table S2. Cell parameters

	$LiFeSO_4F$	**$Li_{1/2}FeSO4F$**	**$FeSO_4F$**
Spacegroup	*P-1*	*P-1*	*C2/c*
Z	*2*	2	4
a / Å	*5.17526 (0.00004)*	5.14274 (0.00006)	7.31019 (0.00014)
b / Å	*5.49008 (0.00003)*	5.30174 (0.00007)	7.07042 (0.00006)
c / Å	*7.22510 (0.00004*	7.32838 (0.00008)	7.30835 (0.00014)
α / °	*106.51204 (0.00035)*	108.82819 (0.00094)	90 (-)
β / °	*107.20097 (0.00036)*	109.40907 (0.00086)	119.74599 (0.00041)
γ / °	*97.85288 (0.00033)*	94.30349 (0.00074)	90 (-)
V /Å^3	*182.476(0.002)*	174.614(0.004)	327.967(0.010)
V/Z /Å^3	*91.238 (0.001)*	87.307(0.002)	81.9918 (0.0034)

Table S3. Atomic positions for *tavorite* type $LiFeSO_4F$. Occupancies and b-factors were taken from the literature and kept constant.[1] The Li position was not refined.

Atom	Wyckoff site	x	y	z
Li	*2i*	0.27(-)	0.634(-)	0.757(-)
Fe1	*1b*	0(-)	0(-)	0.5(-)
Fe2	*1a*	0(-)	0(-)	0(-)
S1	*2i*	0.32528 (22)	0.63366 (20)	0.25166 (16)
O1	*2i*	0.60429 (48)	0.74943 (38)	0.40859 (36)
O2	*2i*	0.10163 (45)	0.64172 (36)	0.34291 (33)
O3	*2i*	0.31312 (42)	0.35559 (20)	0.15012 (33)
O4	*2i*	0.27026 (39)	0.77352 (39)	0.10354 (33)
F	*2i*	0.12787 (35)	00.90776 (37)	00.75663 (28)

Table S4. Atomic positions for $Li_{1/2}FeSO_4F$. The occupancies were set to 1 (except for Li which was set to 0.5). An overall b-factor was refined to 1.24635 (0.02571). The Li position was not refined.

Atom	Wyckoff site	x	y	z
Li	*2i*	0.27(-)	0.634(-)	0.757(-)
Fe1	*1b*	0(-)	0(-)	0.5(-)
Fe2	*1a*	0(-)	0(-)	0(-)
S1	*2i*	0.33959(32)	0.63391(32)	0.25756(28)
O1	*2i*	0.61369(66)	0.75259(62)	0.40332(50)
O2	*2i*	0.30841(71)	0.34102(73)	0.15667(53)
O3	*2i*	0.30973(61)	0.78311(58)	0.11693(49)
O4	*2i*	0.30973(61)	0.78311(58)	0.11693(49)
F	*2i*	0.12044(54)	0.91221(49)	0.75195 (41)

Table S 5. Atomic positions for $FeSO_4F$. The occupancies were set to 1. An overall b-factor was refined to 0.36973 (0.01515).

Atom	Wyckoff site	X	y	z
Fe	*4d*	0.25(-)	0.25(-)	0.5(-)
S	*4e*	0(-)	0.63511(14)	0.25 (-)
F	*4e*	0 (-)	0.16276 (23)	0.25 (-)
O1	*8f*	0.34216(36)	0.00834(19)	0.08858(37)
O2	*8f*	0.41312(65)	0.26282(25)	0.34575(69)

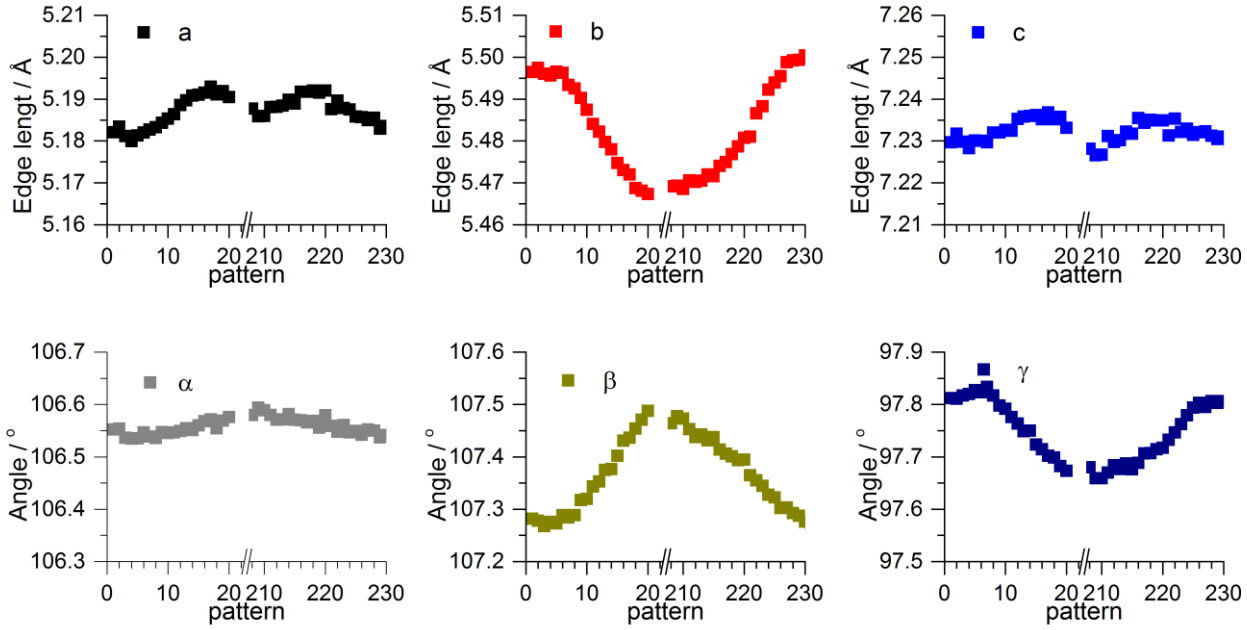

Figure S3. Change in cell parameters for Li_xFeSO_4F (1<x<0.85) from *in operando* XRD at C/50 (10 mg cm^{-2}).

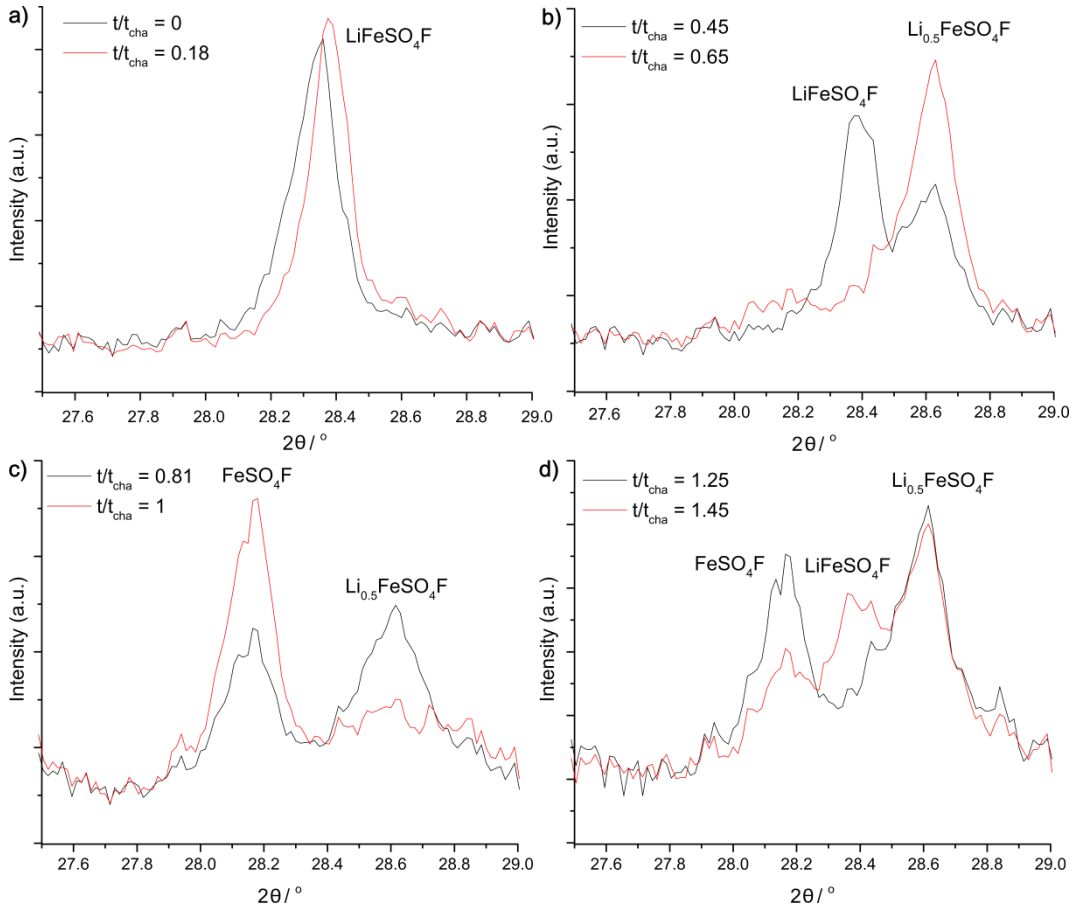

Figure S4. Zoomed in areas with characteristic peaks for Li_xFeSO_4F with different average lithium contents *x*. a) 1<*x*<0.86 during charge, showing an almost invariant intensity and a slight broadening and shift in the Bragg position for the start phase, indicating solid solution behavior in this region. b) 0.65<*x*<0.49 during charge, showing a typical biphasic transition from the fully lithiated to the half lithiated phase with no solid solution region observed within the experimental resolution for $Li_{0.5}FeSO_4F$. c) 0.36<x<0.22 during charge, showing typical biphasic transformation also from $Li_{0.5}FeSO_4F$ to $FeSO_4F$. d) 0.41<*x*<0.57 on discharge, showing the coexistence of all three Li_xFeSO_4F (*x* = 1, 0.5, 0) in contrast to what was observed during charge (shown in b).

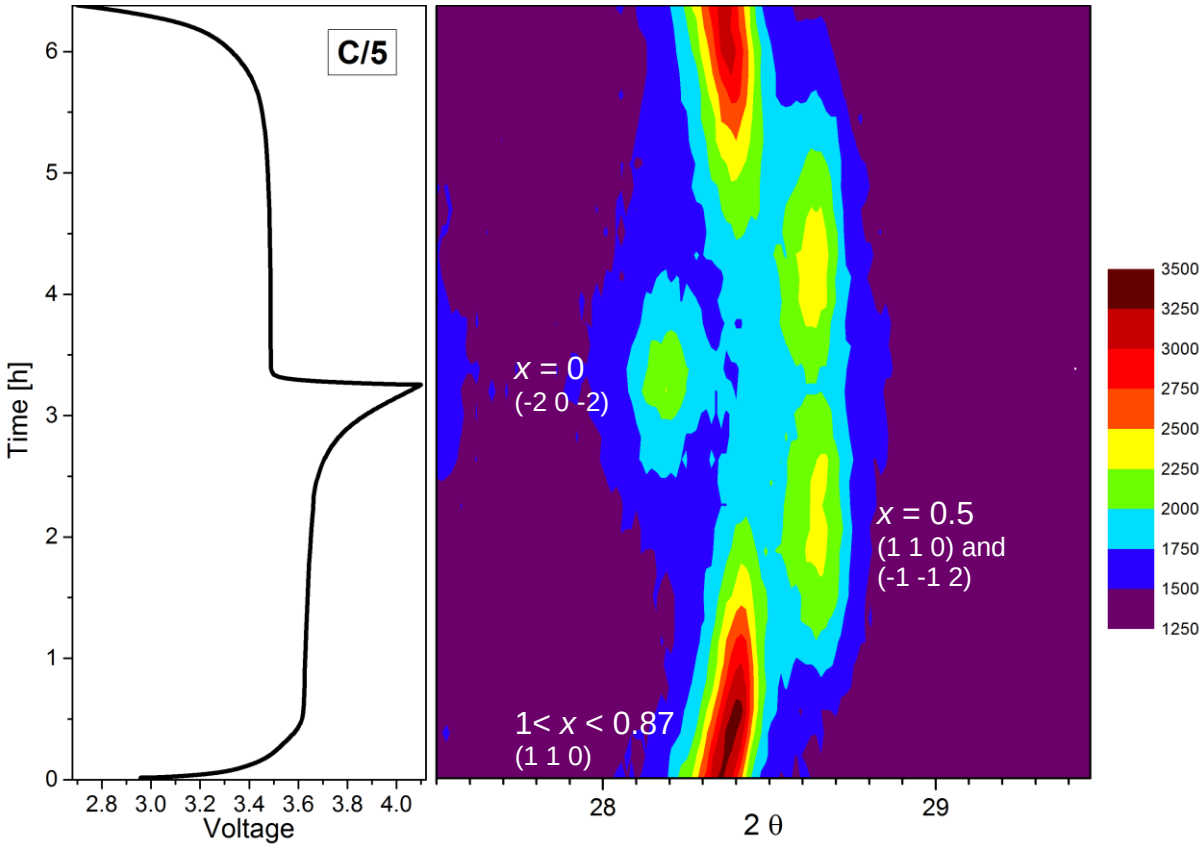

Figure S5. *In operando* XRD at C/5 (10 mg cm^{-2} material loading), showing a solid solution region only for the start phase with 1<x<0.87 in Li_xFeSO_4F. The solid solution region can be seen as a shift in the Bragg position of the (1 1 0) reflection for the lithiated phase, but not in the (1 1 0) and (-1 -1 2) reflections for the intermediate phase $Li_{0.5}FeSO_4F$ or the (-2 0 2) reflection for the end phase.

III. Mössbauer hyperfine parameters

Table S6. Mössbauer hyperfine parameters, obtained by Lorentzian peak fitting to the spectra of tavorite Li_xFeSO_4F with x=1, 0.43, and 0.07. CS = center shift (the sum of the true isomer shift and the second-order Doppler shift, QS= Quadrupole splitting, w= Line width, I =Intensity, ○ = Value fixed during the fitting process

	Fe^{2+}-1				**Fe^{2+}-2**				**Fe^{3+}-1**				**Fe^{3+}-2**			
x in Li_xFeSO_4	CS [mm/s	QS [mm/s	w [mm/s	I [%]	CS [mm/s	QS [mm/s	w [mm/s	I [%]	CS [mm/s	QS [mm/s	w [mm/s	I [%]	CS [mm/s	QS [mm/s	w [mm/s	I [%]
1	1.31(1)	2.83(1)	0.12(1)	47(2)	1.31(1)	2.15(1)	0.14(1)	53(2)	-	-	-	-	-	-	-	-
0.43	1.27(1)	2.69(3)	0.18(2)	18(4)	1.24(1)	2.26(3)	0.20(2)	25(4)	0.48(1)	0.26(3)	0.16(3)	26(6)	0.50(1)	0.62(3)	0.17(1)	31(6)
0.07	1.3 ○	2.5 ○	0.2 ○	6.5(6)	-	-	-	-	0.49(1)	0.58(3)	0.17(1)	53(12)	0.49(1)	0.22(3)	0.16(3)	41(13)

IV. Additional electrochemical characterization

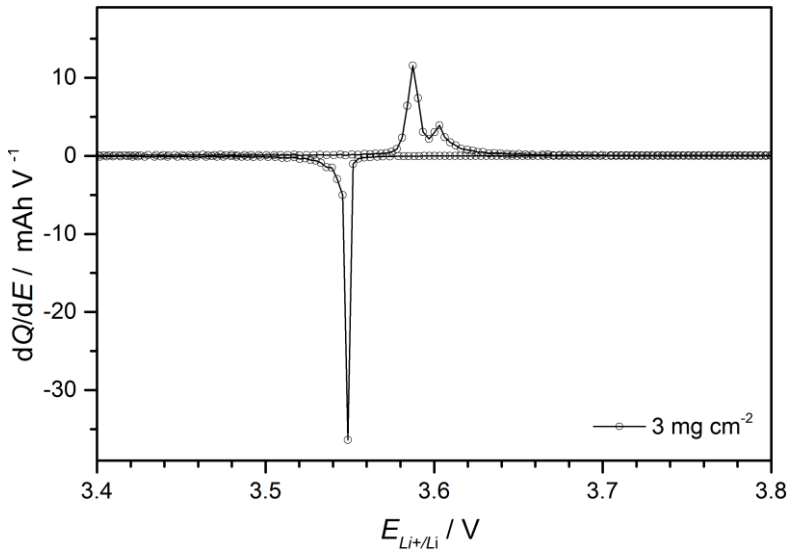

Figure S6. Differential capacity relative the recorded potential for a representative galvanostatic cycling profile. The data was processed and compacted using the EC-lab® software.

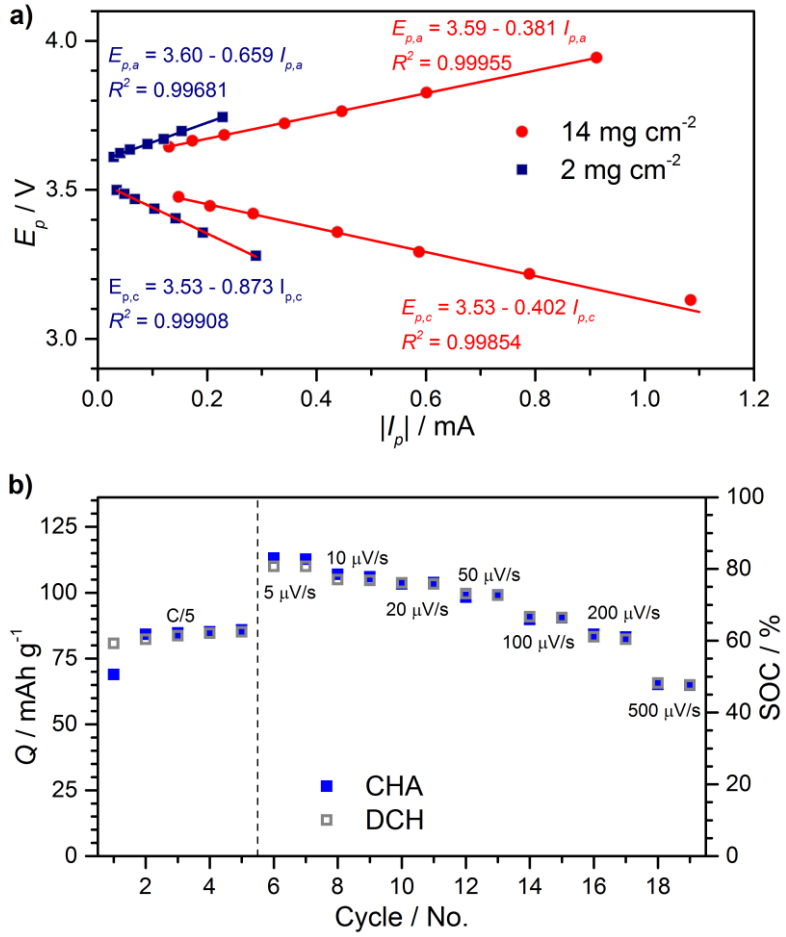

Figure S7. a) The shift in peak potential as a function of the peak current with different mass loadings. The geometric area was 0.785 cm^2 and the cell resistance was obtained from the slopes of the fitted lines. b) The capacity retention during cyclic voltammetry measurements

V. Statistical variation of accessible capacity at C/5

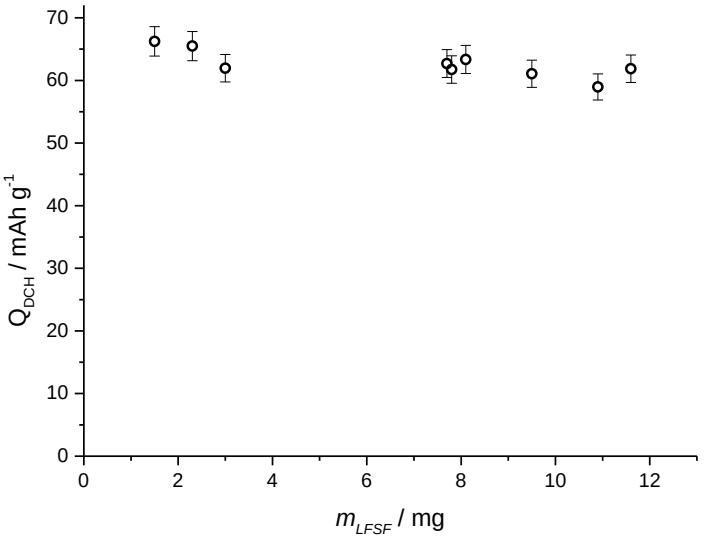

Figure S8. The discharge capacity cycle relative to the active material mass loading. No strong correlation between mass loading and discharge capacity was observed. The discharge capacity was measured at the second cycle of the battery, at a rate of C/5.

VI. Polarizaion during *in operando* XRD

Table S7. Voltage difference between charge and discharge at different rates E_{cha} and E_{dch} was extracted from the maximum derivative of the charge as a function of voltage (dQ/dE).

m / mg cm^{-2}	Rate / h^{-1}	E_{cha} / $V_{Li+/Li}$	E_{dch} / $V_{Li+/Li}$	ΔE / $V_{Li+/Li}$
3	C/50	3.595[a]	3.549	**0.046**
10	C/50	3.595[a]	3.549	**0.046**
10 (cycled)	C/50	3.627	3.496	**0.131**
3	C/5	3.599	3.524	**0.075**
10	C/5	3.624	3.508	**0.116**
10	C/3.5	3.638	3.498	**0.140**
10	C/2	3.681	3.467	**0.214**

[a] Average value for the two voltage plateaus observed during charge.

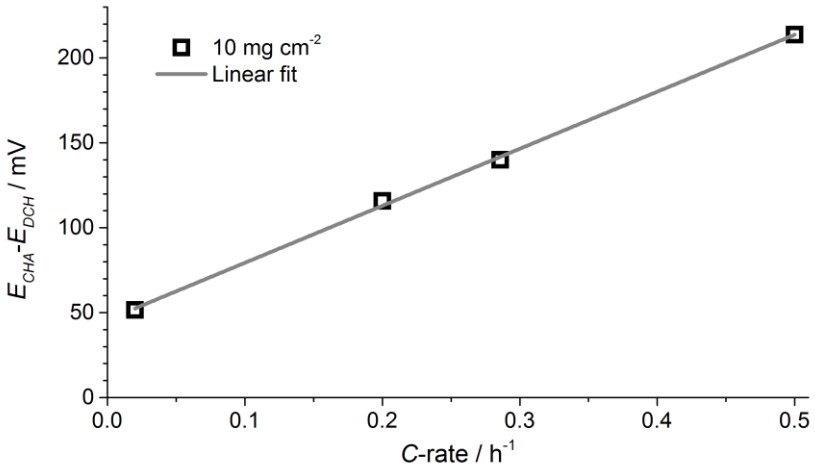

Figure S9. The difference between the charge and discharge plateaus (extracted from the maximum derivatives) relative the applied C-rate.

VII. References

[1] B. C. Melot, G. Rousse, J.-N. Chotard, M. Ati, J. Rodríguez-Carvajal, M. C. Kemei, J.-M. Tarascon, *Chem. Mater.* **2011**, *23*, 2922–2930.

[2] C. Ocampo, R. Oliver, E. Armelin, C. Alemán, F. Estrany, *J. Polym. Res.* **2006**, *13*, 193–200.

[3] K. Hayamizu, *J. Chem. Eng. Data* **2012**, *57*, 2012–2017.